Optical dating of charcoal kiln remains from WWII: a test of accuracy

Karimi Moayed, N.; Vandenberghe, D.; Deforce, K.; Kaptijn, E.; Lambers, K.; Verschoof-van der Vaart, W.; ... ; De Grave, J.

Quaternary Geochronology 83 (2024) 101582

Contents lists available at ScienceDirect

Quaternary Geochronology

journal homepage: www.elsevier.com/locate/quageo

Book review

Optical dating of charcoal kiln remains from WWII: A test of accuracy

Nasrin Karimi Moayed [a,*], Dimitri Vandenberghe [a], Koen Deforce [b,c], Eva Kaptijn [d], Karsten Lambers [e], Wouter Verschoof-van der Vaart [e], Wim De Clercq [b], Johan De Grave [a]

[a] Laboratory of Mineralogy and Petrology, Department of Geology, Ghent University, Krijgslaan 281 (S8), B-9000 Gent, Belgium
[b] Department of Archaeology, Ghent University, Sint-Pietersnieuwstraat 35, B-9000 Brussels, Belgium
[c] OD Earth and History of Life, Royal Belgian Institute of Natural Sciences, Vautierstraat 29, B-1000 Brussels, Belgium
[d] Het Oversticht, Aan de Stadsmuur 79-83, Postbus 531 | 8000 AM Zwolle, the Netherlands
[e] Faculty of Archaeology, Leiden University, Einsteinweg 2, Leiden 2333, the Netherlands

ARTICLE INFO

Keywords:
Charcoal kilns
OSL dating
Early modern period
Accuracy
Precision

ABSTRACT

The majority of relic charcoal kilns in Europe are more recent than 1650 CE and cannot be precisely dated using radiocarbon dating (^{14}C). Quartz-based optically stimulated luminescence (OSL) dating of the sediments associated with the kiln remains has been suggested as a viable alternative. Owing to the lack of reliable and sufficiently precise independent age information, however, it remains to be established whether OSL dating can yield accurate ages for post-1650 CE features. This is explicitly investigated in this study by applying a commonly adopted quartz OSL methodology to three relic charcoal kilns which are known to have been constructed and operated between December 1941 and March/April 1942 CE.

We first document the quartz luminescence characteristics and show through procedural tests that the adopted single-aliquot regenerative dose procedure should be appropriate for equivalent dose determination. Four samples collected from the uppermost part of the charcoal-rich layers in the three features yield the youngest optical ages and are considered coeval. Their average age is 1928 ± 13 CE (95% probability), which matches the independent age reasonably well. The precision associated with the individual OSL ages ranges between 7 and 14% (1 sigma total uncertainty) and it might ideally be possible to establish relative chronologies with a higher time resolution. Finally, we briefly discuss our entire set of OSL ages in relation to future strategies for sampling charcoal kilns remains. In general, we conclude that OSL dating can be particularly advantageous to help resolving chronometric issues that pertain to post-1650 CE relic charcoal kilns.

1. Introduction

Charcoal production in above-ground kilns was widespread in NW Europe during early-Modern (15th - late 18th century) and Modern (late 18th century – present) times (Gale, 2003; Deforce et al., 2021a). The remains (or relics) of these charcoal kilns are increasingly studied to inform about former forest composition and exploitation (Ludemann, 2003, 2010; Nelle, 2003; Deforce et al., 2013, 2021b) as well as settlement dynamics (Groenewoudt and Spek, 2016; Deforce et al., 2021a), associated economic activities (Raab et al., 2015; Rutkiewicz et al., 2017; Olesen, 2019), and to study long and short term effects of charcoal production on ecosystems (Foster et al., 2003; Willis and Birks, 2006). All these studies require a temporal framework for charcoal production. Such chronologies are most commonly established using ^{14}C dating of charcoal fragments, which are abundant in the relic kilns. It is well known, however, that the applicability of ^{14}C dating is limited for features that are more recent than ~1650 CE owing to De Vries and Suess effects (Stuiver, 1961; Tans et al., 1979). The calibrated probability distributions for post-1650 CE radiocarbon ages are so broad that their ages cannot be differentiated (e.g., Deforce et al., 2021a). Most NW European charcoal kilns, however, date from exactly this post-1650 CE period, as a result of the increasing need for fuel during the initial stages of industrialization, before the large-scale exploitation of coal (Hardy and Dufey, 2012; Raab et al., 2015).

Previous research (Karimi-Moayed et al., 2020, 2022, 2023) has explored the potential of quartz-based OSL dating as an alternative to ^{14}C-dating for determining the age of relic charcoal kilns. Through comparison with ^{14}C-dates and historical evidence (where available), it was shown that - for pre-1650 CE features - the approach can yield accurate ages, with a precision that is comparable or better than ^{14}C. For

* Corresponding author.
E-mail address: nasrin.karimimoayed@ugent.be (N. Karimi Moayed).

https://doi.org/10.1016/j.quageo.2024.101582
Received 14 November 2023; Received in revised form 15 May 2024; Accepted 23 June 2024
Available online 28 June 2024

features that postdate 1650 CE, however, the considerable limits on the precision of the independent age information (covering a range from about 1650 CE to present) did not allow assessing to what extent the OSL dates are truly accurate as well. The present study seeks to explicitly investigate this, by applying the same methodology (Karimi-Moayed et al., 2020, 2022, 2023) to three relatively recent charcoal kiln remains for which the independent age control is tightly constrained to the end of 1941 CE – beginning of 1942 CE.

2. Study site and historical background

The three investigated charcoal kilns are located at "De Ginkel" (52.034°N, 5.74°E), a heath area on an ice-pushed ridge in the southern Veluwe (Central Netherlands; Fig. 1a). De Ginkel has been heathland since at least 1653 CE, according to the oldest surviving map. The subsurface geology consists of fine sand with small amounts of loam, resulting in podzol soil formation. Following the Dutch soil classification both the so-called holtpodzol and haarpodzol soils occur. Written evidence for charcoal burning at this location is provided by several newspaper articles (e.g. "Amerfoortse courant", December 13, 1941 CE (https://resolver.kb.nl/resolve?urn=ddd:010900698:mpeg21:p004); "Het Volk", December 17, 1941 CE (https://resolver.kb.nl/resolve?urn=ddd:011118072:mpeg21:p006); "Nieuwe Venlosche Courant", January 14, 1942 CE (https://resolver.kb.nl/resolve?urn=ddd:010492954:mpeg21:p002)). The articles describe that the Schuurkamp family, consisting of four people, was burning 12 charcoal kilns at that time (i.e. December 1941 CE) and would return to burn another four kilns in the period March–April 1942 CE. This matches the remains of 16 kilns whose locations are indicated on a map (Fig. 1b) and LiDAR image (Fig. 1c) as well as an aerial photograph that was taken by the RAF (Fig. 1d) during airborne landings on September 19, 1944 (as part of the allied military operation "Market Garden" during World War II). Charcoal burning at De Ginkel likely reflects the wartime fuel shortages and increased charcoal demand (e.g., conversion of vehicles to charcoal gas producers during WWII). Apart from constraining the relic charcoal kilns to December 1941 CE – March/April 1942 CE, the newspaper articles also provide insights into, for instance, the practice of charcoal burning. Relevant to this study is the documentation that the charcoal kilns burned for a period of 14 days, after which they were left to cool down for another 14 days.

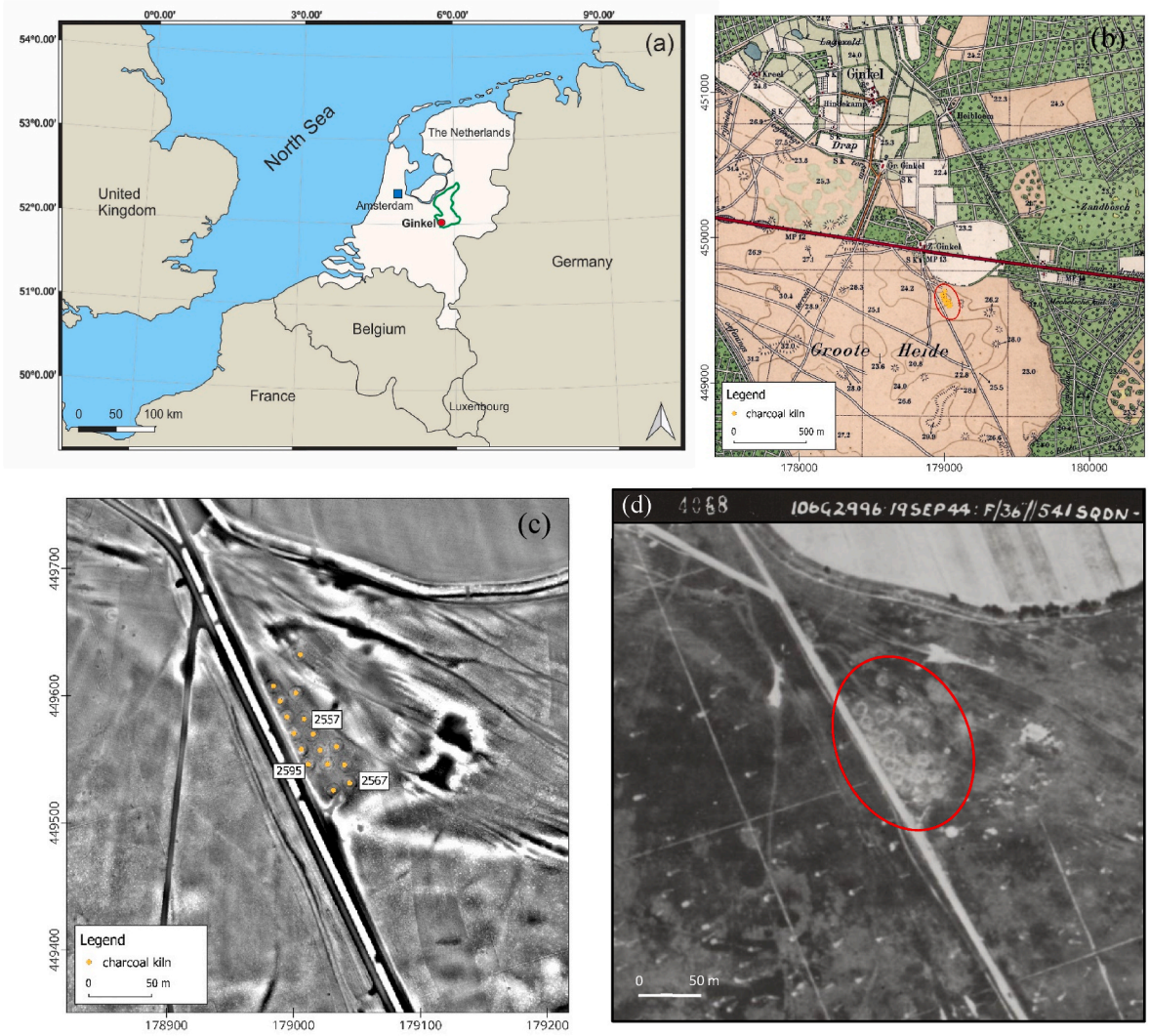

Fig. 1. (a) The green outline marks the remaining Veluwe forest in central Netherlands. The study site (De Ginkel) is located in the southernmost part of the Veluwe forest. (b) A map of De Ginkel (Ede) in the 1940's with the charcoal kilns represented as yellow dots inside a red ellipse (source: topotijdreis). (c) LiDAR map (Simple Local Relief Model visualization - SLRM, Hesse, 2010) showing 16 charcoal kilns at De Ginkel (source: PDOK). (d) Aerial photograph taken by the Royal Air Force (RAF) on September 19, 1944 during the airborne landings at Ginkel (Operation Market Garden). The charcoal kilns are clearly visible within the red ellipse. The white points dotted across the heath are the parachutes of dropped soldiers. (Source: RAF via http://hdl.handle.net/10648/ae307f3a-d0b4-102d-bcf8-003048976d84).

3. Materials and methods

3.1. Field observations and sampling

After burning and harvesting a kiln, a layer with residual charcoal fragments always remains. This layer can be easily recognized in a soil profile, which is used to confirm that a feature identified through LiDAR images corresponds to a relic charcoal kiln. After validation through hand augering, three kilns (features 2557, 2567, and 2595) were selected for sampling. A shallow pit of ~50 × 50 × 50 cm was dug in the estimated center of each kiln. The exposed stratigraphic sequences were similar for all kilns. All (Fig. 2a–c) have a light brown topsoil overlying darker layers rich in charcoal (5–23 cm thick). These charcoal layers rest on lighter sediments (sand or loam). Notably, Ginkel 2557 has a thin orange-brown layer between charcoal and sand. All stratigraphic layers show root penetration.

Though the area experiences yearly World War II commemorations and animal activity (wild boar and rabbits), no macroscopic evidence of recent disturbance was found in the sampled sequences.

Samples for OSL dating were collected by hammering stainless-steel tubes (5 cm diameter, 15 cm long) into the exposures. The sediment immediately surrounding each tube was collected for radionuclide analysis. To evaluate moisture content, undisturbed samples were taken next to each OSL sample using Kopecky rings. Fig. 2 illustrates the sampling of each kiln and the stratigraphic position of the samples is given in Tables 1 and 2. In the following, we denote the darker, charcoal-rich layers with "D", and the (underlying) lighter layers with "L".

Bulk sediment samples (approximately 10 l) were taken from the uppermost charcoal-rich layer of each kiln for complementary radiocarbon dating and anthracological analysis.

3.2. Optically stimulated luminescence dating

The inner material of the OSL tubes was treated with 10% and 33% HCl to remove carbonates, and 10% and 33% H_2O_2 to remove organic matter. Grains from the 125–180 μm fraction were obtained using wet and dry sieving, and then etched with 40% HF for 40 min to remove feldspar and the outer alpha-irradiated rinds of the quartz grains. Finally, the etched fractions were treated with 10% HCl at 50 °C for 30 min to remove any precipitated fluorides, repeatedly rinsed (5 times), dried, and re-sieved on a 125 μm mesh. For luminescence measurements, quartz grains were mounted on the inner 8 or 2 mm of stainless-steel discs using Rüsch Silkospray ("large" and "small" aliquots, respectively).

The luminescence measurements were performed with two automated Risø TL/OSL readers. Both are equipped with blue LEDs delivering a power (at 100%) of approximately either 35 mW/cm^2 or 84 mW/cm^2 at the sample position, and IR LEDS (120 mW/cm^2 and 160 mW/cm^2). All signals were detected through a 7.5 mm Hoya U-340 UV filter. Laboratory irradiations were performed using beta-sources mounted on the readers delivering ~0.054 and 0.076 Gy/s to sand-sized quartz on stainless steel discs. Details on the luminescence measurement facilities used in this study can be found in Karimi-Moayed (2023) and references therein.

The single-aliquot regenerative-dose (SAR) protocol was used for equivalent dose (D_e) determination (Murray and Wintle, 2000, 2003). Preheating was for 10 s at a temperature in between 160 and 280 °C, while a cut heat to either 160 °C or a temperature that tracks the preheat by minus 20 °C was adopted. Stimulation with blue diodes was for 38.5 s at 125 °C, and the first 0.31 s of the decay curve (minus a background evaluated from the subsequent 0.77s of stimulation) was used in the calculations. Each measurement of the response to the test dose (2 Gy in all experiments) was followed by a stimulation with the blue diodes for 38.5 at 280 °C. Each aliquot was tested for the presence of feldspar through the OSL IR depletion ratio (Duller, 2003). To assess the suitability of the laboratory measurement protocol, dose recovery tests were performed. In these tests, natural aliquots were bleached for two times 250 s at room temperature, with a 10 000 s pause in between. They were then given a laboratory dose equal to the estimated D_e and measured as outlined above.

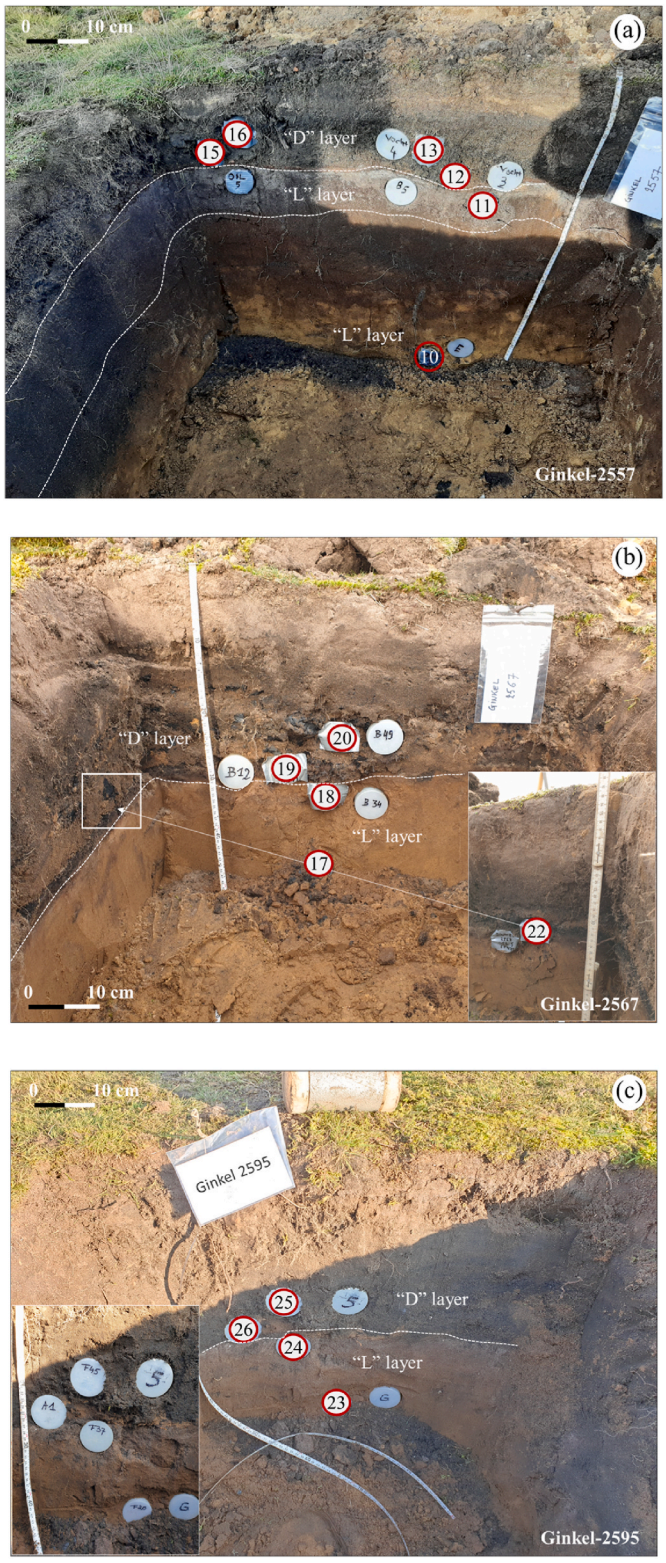

Fig. 2. Photographs of features 2557 (a), 2567 (b) and 2595 (c) at De Ginkel. The OSL samples from "D" and "L" layers in Table 1 are highlighted on these photos. Bulk samples for ^{14}C and anthracological analysis were collected from the dark charcoal-rich 'D' layer.

Table 1
Specific radionuclide activities, measured water contents at the time of sampling (W_n) and at saturation (W), the calculated fraction of saturation (F) to which the time-averaged water content is assumed to correspond, and the effective (beta + gamma) dose rates. See the main text for details.

Feature	*Depth (cm)*	*Material*	*Lab code*	*^{234}Th (Bq kg^{-1})*	*^{226}Ra (Bq kg^{-1})*	*^{210}Pb (Bq kg^{-1})*	*^{232}Th (Bq kg^{-1})*	*^{40}K (Bq kg^{-1})*	*W_n*	*W*	*F*	*Eff. Dose rate (Gy/ka)*
Ginkel (2557)	**15**	**D**	**214316**	**7.3 ± 1.3**	**8.0 ± 0.3**	**22.0 ± 1.1**	**7.0 ± 0.2**	**189 ± 3**	**0.061**	**0.524**	**0.12 ± 0.01**	**1.01 ± 0.02**
	15	**D**	**214313**	**5.0 ± 0.8**	**8.0 ± 0.4**	**18.9 ± 1.2**	**7.4 ± 0.2**	**204 ± 2**	**0.061**	**0.524**	**0.12 ± 0.01**	**1.00 ± 0.02**
	20	**D**	**214315**	**3.4 ± 1.1**	**7.5 ± 0.2**	**12.5 ± 1.4**	**6.7 ± 0.3**	**194 ± 2**	**0.107**	**0.637**	**0.17 ± 0.05**	**0.82 ± 0.01**
	20	**D**	**214312**	**3.6 ± 1.3**	**7.4 ± 0.2**	**7.3 ± 1.2**	**7.4 ± 0.2**	**197 ± 3**	**0.107**	**0.637**	**0.17 ± 0.05**	**0.77 ± 0.01**
	25	L	214311	5.8 ± 0.4	7.2 ± 0.3	8.2 ± 0.6	7.1 ± 0.2	191 ± 2	0.075	0.292	0.26 ± 0.04	0.80 ± 0.01
	65	L	214310	5.7 ± 1.0	7.6 ± 0.3	4.6 ± 1.1	7.2 ± 0.2	238 ± 3	0.058	0.282	0.21 ± 0.01	0.91 ± 0.02
Ginkel (2567)	**25**	**D**	**214320**	**7.4 ± 1.2**	**8.4 ± 0.4**	**10.0 ± 1.3**	**7.7 ± 0.3**	**210 ± 3**	**0.063**	**0.333**	**0.19 ± 0.02**	**0.91 ± 0.02**
	25	**D**	**214322**	**6.5 ± 1.2**	**7.7 ± 0.2**	**7.0 ± 1.1**	**7.5 ± 0.2**	**210 ± 4**	**0.327**	**0.572**	**0.57 ± 0.21**	**0.66 ± 0.01**
	30	**D**	**214319**	**5.1 ± 1.6**	**7.8 ± 0.3**	**8.9 ± 1.1**	**7.6 ± 0.3**	**218 ± 3**	**0.327**	**0.572**	**0.57 ± 0.21**	**0.70 ± 0.01**
	35	L	214318	8.2 ± 1.5	7.8 ± 0.3	9.2 ± 1.3	7.7 ± 0.2	208 ± 3	0.093	0.295	0.32 ± 0.07	0.87 ± 0.01
	45	L	214317	8.1 ± 1.2	7.5 ± 0.3	8.0 ± 1.4	7.6 ± 0.2	223 ± 3	0.093	0.295	0.32 ± 0.07	0.89 ± 0.02
Ginkel (2595)	**22**	**D**	**214325**	**6.7 ± 1.4**	**7.6 ± 0.3**	**9.1 ± 1.2**	**7.2 ± 0.2**	**216 ± 3**	**0.579**	**0.876**	**0.66 ± 0.17**	**0.57 ± 0.01**
	27	**D**	**214326**	**6.7 ± 1.4**	**7.6 ± 0.4**	**9.1 ± 1.2**	**7.2 ± 0.2**	**216 ± 3**	**0.579**	**0.876**	**0.66 ± 0.17**	**0.57 ± 0.01**
	32	L	214324	9.5 ± 1.4	7.4 ± 0.3	8.7 ± 1.1	7.6 ± 0.2	215 ± 3	0.103	0.348	0.30 ± 0.08	0.87 ± 0.02
	45	L	214323	4.5 ± 1.8	7.8 ± 0.2	5.2 ± 1.1	7.8 ± 0.2	209 ± 3	0.103	0.348	0.30 ± 0.08	0.79 ± 0.01

Table 2
Calculated total dose rates, D_e values, OSL ages, and random (σ_r), systematic (σ_s), and total uncertainties (σ_{tot}). In the last column, the OSL ages are expressed as ages CE (±2σ total uncertainties). The total dose rate includes the contributions from internal radioactivity and cosmic radiation. The number of aliquots used for D_e-determination is indicated between parentheses in the subscript. All uncertainties related to dosimetry and D_e data are random. All uncertainties represent 1 sigma (except for those associated with the ages CE in last column). Samples were ranked according to depth below the surface level, with "D" and "L" denoting darker charcoal-rich and lighter-colored layers, respectively. Results for samples collected from the "D"-layers are highlighted in bold.

Feature	*Depth (cm)*	Material	*Lab code*	*Total dose rate (Gy ka^{-1})*	*D_e (Gy)*	*Age (ka)*	*σ_r (%)*	*σ_{sys} (%)*	*σ_{tot} (%)*	*Age (CE) (±2σ)*
Ginkel (2557)	**15**	**D**	**214316**	**1.30 ± 0.02**	**0.107 ± 0.004$_{(39)}$**	**0.08 ± 0.01**	**3.85**	**5.72**	**6.89**	**1939 ± 11**
	15	**D**	**214313**	**1.29 ± 0.02**	**0.14 ± 0.01$_{(41)}$**	**0.11 ± 0.01**	**7.62**	**5.74**	**9.54**	**1912 ± 21**
	20	**D**	**214315**	**1.13 ± 0.02**	**0.13 ± 0.01$_{(43)}$**	**0.12 ± 0.01**	**4.69**	**6.42**	**7.95**	**1905 ± 18**
	20	**D**	**214312**	**1.05 ± 0.02**	**0.13 ± 0.01$_{(38)}$**	**0.12 ± 0.01**	**4.96**	**6.48**	**8.16**	**1901 ± 20**
	25	L	214311	1.06 ± 0.01	0.9 ± 0.1$_{(22)}$	0.85 ± 0.10	10.47	5.96	12.04	1175 ± 204
	65	L	214310	1.13 ± 0.02	11.8 ± 1.6$_{(4)}$	10.4 ± 1.6	13.99	5.73	15.12	−8408 ± 3153
Ginkel (2567)	**25**	**D**	**214320**	**1.17 ± 0.02**	**0.108 ± 0.003$_{(44)}$**	**0.09 ± 0.01**	**3.55**	**5.80**	**6.80**	**1929 ± 13**
	25	**D**	**214322**	**0.93 ± 0.02**	**0.15 ± 0.01$_{(47)}$**	**0.16 ± 0.02**	**6.01**	**12.27**	**13.66**	**1860 ± 44**
	30	**D**	**214319**	**0. 96 ± 0.01**	**0.35 ± 0.03$_{(43)}$**	**0.36 ± 0.05**	**8.13**	**12.41**	**14.84**	**1660 ± 107**
	35	L	214318	1.11 ± 0.02	2.2 ± 0.2$_{(24)}$	1.99 ± 0.22	9.27	6.10	11.09	28 ± 442
	45	L	214317	1.12 ± 0.02	5.2 ± 0.9$_{(4)}$	4.62 ± 0.81	16.56	6.09	17.64	−2597 ± 1629
Ginkel (2595)	**22**	**D**	**214325**	**0.85 ± 0.01**	**0.101 ± 0.003$_{(46)}$**	**0.12 ± 0.02**	**3.17**	**13.64**	**14.00**	**1903 ± 33**
	27	**D**	**214326**	**0.83 ± 0.01**	**0.14 ± 0.01$_{(45)}$**	**0.16 ± 0.02**	**5.04**	**13.84**	**14.73**	**1859 ± 48**
	32	L	214324	1.13 ± 0.02	0.8 ± 0.1$_{(24)}$	0.69 ± 0.09	10.88	6.29	12.57	1332 ± 173
	45	L	214323	1.03 ± 0.02	5.2 ± 0.4$_{(4)}$	5.07 ± 0.54	8.50	6.31	10.59	−3054 ± 1074

The sediment collected for radionuclide analysis was dried, pulverized, and homogenized. A subsample of the powder was then cast in wax and stored for at least one month before being measured using a low-level extended energy-range HPGe gamma-ray spectrometer (Hossain, 2003; Vandenberghe, 2004; Karimi-Moayed, 2023). Specific activities were converted to dose rates using conversion factors derived from the nuclear data tabulated by Adamiec and Aitken (1998). A factor of 0.90 (±5 % relative uncertainty) was adopted to correct the external beta dose rates for the effects of attenuation and etching (Mejdahl, 1979; Aitken, 1985). The correction for the effect of moisture was performed as outlined by Aitken (1985), in which the time-averaged moisture content is obtained by multiplying the water content at saturation (measured in the lab and denoted by "W") by the fraction of saturation to which the assumed water content corresponds (denoted by "F"). We assumed that the time-averaged water content corresponds to the water content at the time of sampling. The difference between the natural water content and either a lower limit of 5% or an upper limit equal to the content at saturation, was considered to represent the 2-sigma uncertainty on our estimates, which was then propagated to the uncertainty on "F" (Table 1). An internal dose rate in quartz of 0.013 ± 0.003 Gy ka^{-1} was adopted (Vandenberghe et al., 2008), and the contribution of cosmic rays was calculated following Prescott and Hutton (1994) to

which a 15% relative uncertainty was assigned.

3.3. Anthracological analysis and radiocarbon dating

The bulk samples were wet-sieved through a 0.5 mm mesh, and air-dried. For each kiln, at least 100 charcoal fragments were then randomly selected and studied using reflected light microscopy (50-500x) and darkfield illumination. The identifications were based on the description of wood anatomical characters by Schoch et al. (2004) and the reference collection of artificially charred wood held at the Royal Belgian Institute of Natural Sciences in Brussels.

From the identified fragments, those with the lowest potential age at the time of charring were then selected for radiocarbon dating, i.e. twigs or taxa with a low maximal expected age to avoid a potential old wood effect. Following standard acid-base-acid ("ABA") pre-treatment, the samples were combusted to CO_2 and transformed into graphite, and radiocarbon concentrations were measured using a MICADAS AMS instrument at the Royal Institute for Cultural Heritage, Brussels, Belgium (Boudin et al., 2015). Results were calibrated using CALIBomb (Reimer and Reimer, 2023) and the IntCal20 calibration curve (Reimer et al., 2020).

4. Experiments and results

4.1. OSL dating

4.1.1. Luminescence characteristics

Fig. 3a shows a typical natural and regenerated OSL decay curve for a large (8 mm diameter) aliquot of sample GLL-214313, which was taken from the dark charcoal-rich ("D") layer in feature Ginkel-2557. The signals are clearly distinguishable from the background level and decay rapidly with stimulation time. Comparison with calibration quartz (inset to Fig. 3a, dashed line) indicates that the signals from our samples (solid line) are dominated by the fast component. The growth of the regenerated signal with dose (Fig. 3b) can be well represented by a single saturating exponential function and is linear up to a few Gy (inset to Fig. 3b). The dose response curve passes through the origin, indicating that the recuperation is negligible (open square in Fig. 3b), and it is possible to remeasure a regenerated dose point, implying that sensitivity changes occurring throughout the SAR measurement sequence are accurately corrected for (overlying solid and open circles in Fig. 3b). This behavior is representative of all samples taken from the "D"-layers, as summarized in Fig. S1 for all aliquots used for ED determination (n = 431). Within 1 sigma analytical uncertainty, most individual values for recuperation do not exceed 5% of the corrected natural OSL signal, as suggested as a possible criterion for acceptance by Murray and Wintle (2000); on average (±1 standard error), recuperation amounts to 0.4 ± 0.2% (Fig. S1a). Similarly, about 97% of the aliquots (n = 419) have a recycling ratio between 0.90 and 1.10, with an overall average of 1.015 ± 0.003 (Fig. S1b). All aliquots yield OSL IR depletion ratios that are consistent with no sensitivity to infrared stimulation (Fig. S1c), indicating that there is no feldspar contamination (Duller, 2003). Comparable finds were made for the samples collected from the lighter "L" layers (Fig. S2).

To assess the suitability of SAR measurement parameters for equivalent dose (D_e) determination, we first investigated the dependence of D_e on preheat temperature. For one sample (e.g., GLL-214320, Fig. 4a and b), three fresh large (8 mm) aliquots were measured at each of seven different preheat temperatures in the range of 160 °C–280 °C. D_e remained independent of preheat temperatures up to 260 °C. Across the entire temperature range, recycling ratios fall within 0.90–1.10, and recuperation remains well below 5% of the corrected natural signal. The results for the rest of the features are summarized in Fig. S3.

This experiment was then repeated for one sample in each feature, but this time through a dose recovery test (see §3.2). The results are summarized in Fig. 4c,d and Fig. S4. Within 1 sigma uncertainty, and regardless of preheat temperature, most ratios do not deviate by more than 5% from unity. Broadly similar observations were made for samples collected from the "L" layers in each feature (Fig. S5).

For D_e determination, we selected a 10s-preheat at 200 °C and 240 °C and a cut heat to 160 °C for the "D" and "L" samples, respectively. The overall dose recovery ratios (±1 standard error) obtained under these conditions for the "D" and "L" samples are 0.99 ± 0.01 (n = 9) and 1.03 ± 0.01 (n = 9).

4.1.2. Equivalent doses

For each sample that was collected from a "D"-layer, 48 replicate D_e measurements were made using small (2 mm) aliquots. A smaller number (in between 4 and 24) of small aliquots were measured for the samples taken from the underlying lighter "L" layers as we considered them less important for the direct timing of charcoal production but were included to help assessing stratigraphic consistency. The results are

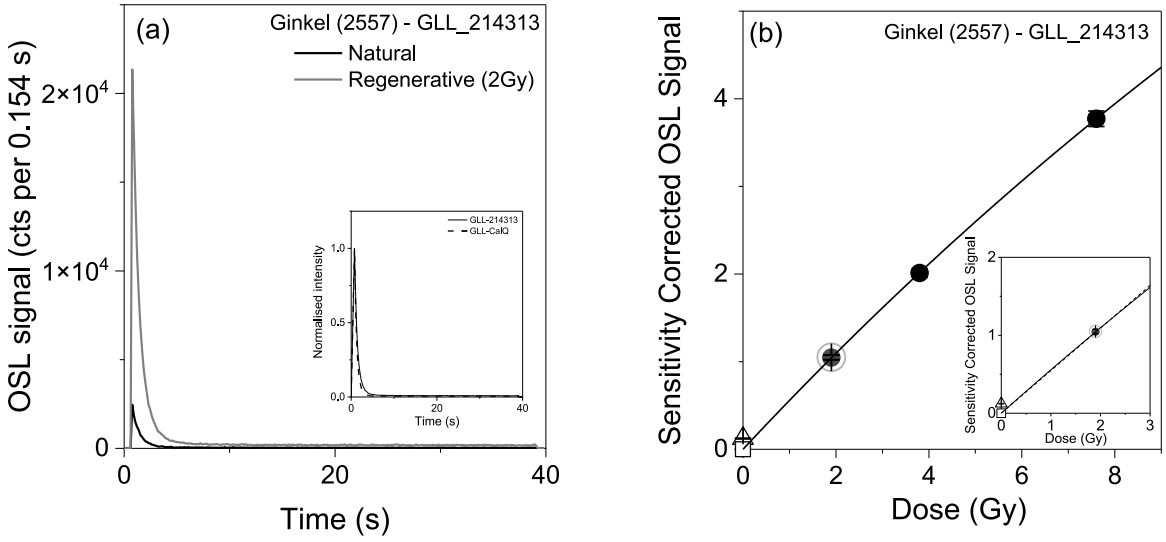

Fig. 3. (a) Natural and regenerated OSL decay curves (black and grey lines, respectively) for an aliquot of quartz grains extracted from sample GLL-214313. The inset compares the decay of the regenerated OSL signal of the sample with that from calibration quartz (GLL-CalQ). (b) SAR growth curve for an aliquot of the same sample, with recycling and recuperation points (open circle and square, respectively), and a single saturating exponential function fitted to the regenerated data (solid circles). The natural signal intersects with the linear region of the dose response curve (inset).

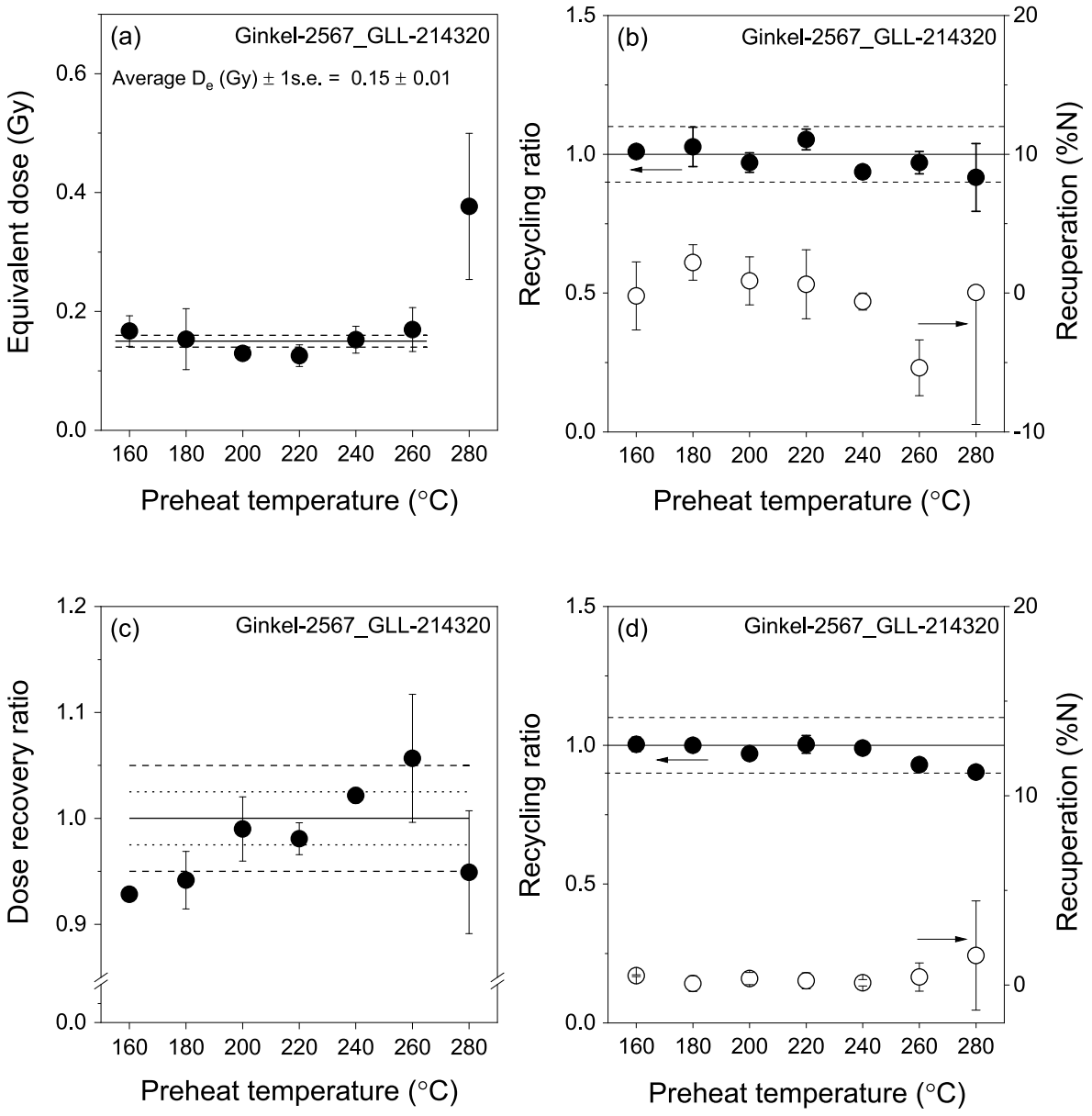

Fig. 4. Dependence of equivalent dose (D_e) (a) and dose recovery ratio (c) on preheat temperature for sample GLL-214320. Each data point represents the average (±1 standard error; 1 s.e.) of 3 measurements. The dashed and dotted lines in Figure (a) represent the average ± 1 s.e. over the 160–260 °C temperature range. The dashed and dotted lines (eye guides) in Figure (c) bracket a 2.5% and 5% deviation of the ratio from unity (solid line). Figures b,d illustrate the corresponding recycling and recuperation.

shown as histograms in Fig. 5. A graph of D_e versus uncertainty above each histogram visualizes the precision by which each individual value was determined. We applied a criterion in which D_e values that differed by more than 3 standard deviations (SD) from the average were iteratively rejected (Karimi-Moayed et al., 2020). For the samples collected from the "D"-layers, the distributions of accepted D_e values exhibit relative standard deviations (RSD) ranging from 19% to 52%. Except for sample GLL-214313, there seems to be a trend of increasing RSD with depth within the "D" layers. The D_e values for the uppermost samples collected from "L" layers (samples GLL-214311, -18, and −24) show RSDs ranging from 44% to 53%. The D_e values in these "L" samples are significantly higher than those in the "D" sample. The mean (±1 standard error) of the accepted D_e's was used in the calculations (Table 2).

4.1.3. Dose rates

Table 1 summarizes the measured specific radionuclide activities, the water contents at the time of sampling (W_n) and at saturation (W), and the calculated fraction of saturation (F) to which the time-averaged water content is assumed to correspond (see §3.2). The effective dose rates (Tables 1 and 2) were calculated from the present-day conditions.

Most samples yielded comparable specific radionuclide activities with no indication of (significant) radioactive disequilibrium in the ^{238}U decay chain. For some of the samples collected from the dark charcoal-rich layers in kiln Ginkel 2257, however, a significant excess in ^{210}Pb is observed. It appears that this excess is located in the upper 15 cm and rapidly decreases with depth, which may reflect natural fallout. This remains to be established as no samples were collected from (near) the surface, nor at shallower depths in the other kilns. As such, any possible effects on the dose rate (as e.g. in Madsen et al., 2005) were not modelled. As pointed out by Olley et al. (1996), the dose rate derived directly from the decay of ^{210}Pb and its daughters is small.

Table 1 illustrates how the measured natural ("W_n") and saturated ("W") water contents can vary both vertically throughout a profile and between the different profiles (which are all located close to each other,

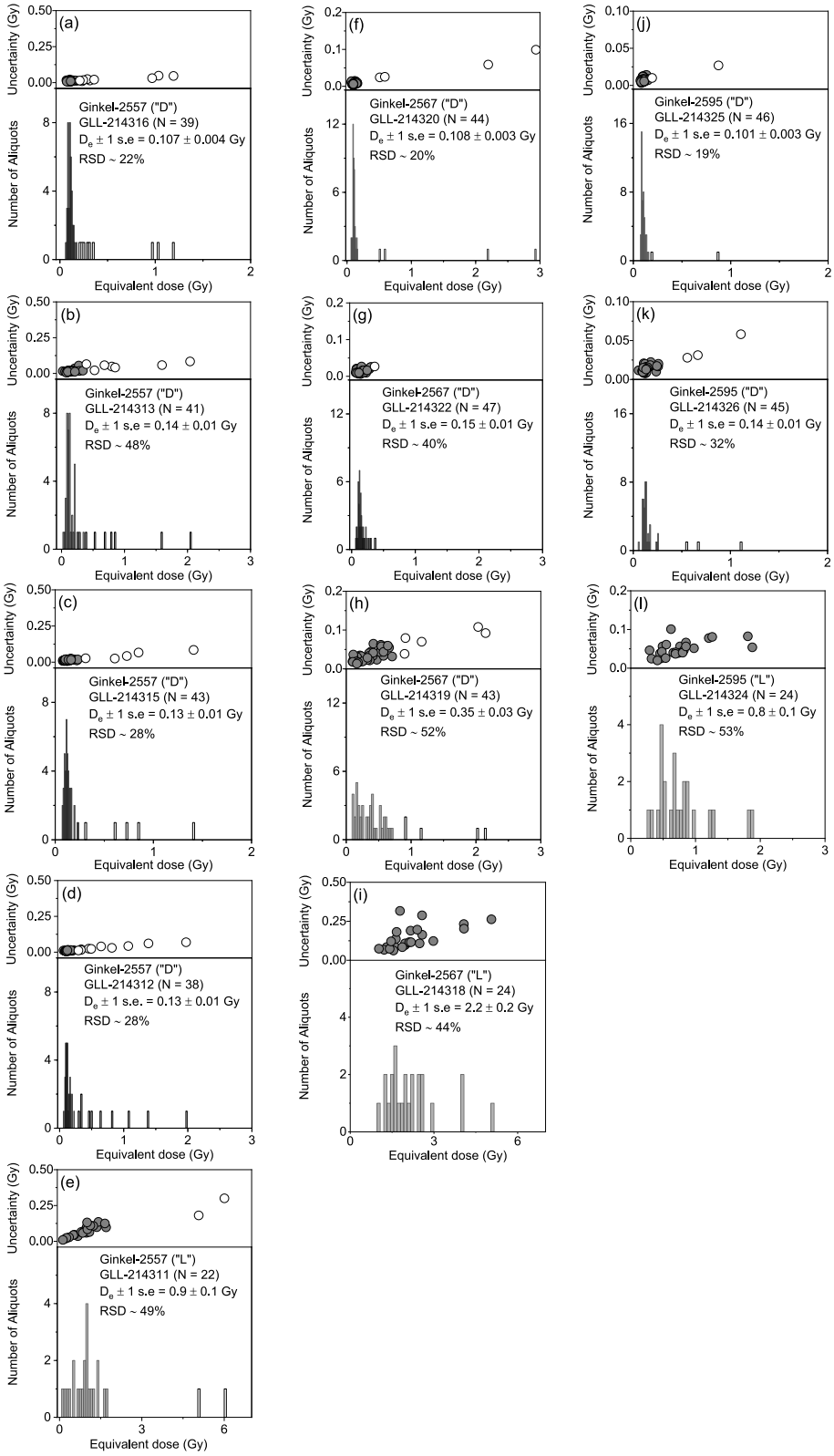

Fig. 5. Small-aliquot (2 mm diameter) distributions of equivalent dose in all "D" and "L" samples from each of the investigated kilns. The median from the distribution of uncertainty (shown above each histogram) was used for binning the data (Lepper et al., 2000). The open bars refer to values that were rejected for calculating the average D_e calculation (see text for details).

i.e. within about 50 m; Fig. 1c). This has also been observed for comparable sequences in this and other areas (Karimi-Moayed et al., 2022, 2023). Especially for the samples from the D-layers, a wide range in as-found wetness and porosity is observed. Given the proximity of the three investigated kilns, this variability can only be explained by very local factors (and not by factors such as overall climate or meteorological conditions). The D-layers are heterogenous in that they consist of larger and smaller pieces of charcoal, and sediment; in addition, charcoal will absorb water, while the clastic component will not. The D-layers can thus have both a higher apparent porosity compared to the underlying loose sediments (L-layers), and one that is variable. This is documented by our dataset, in turn illustrating the importance of collecting additional samples specifically for evaluation of moisture content.

4.1.4. OSL ages

Tables 1 and 2 summarize the analytical results and calculated OSL ages. The uncertainties on the OSL ages were calculated following the procedure outlined in Aitken (1985). For the samples collected from "D" layers, the total uncertainties range from ~7% to ~15% (Table 2). Apart from sample GLL-214313, uncertainties arising from systematic effects contribute most. For samples GLL-214319, -22, −25 and −26, this reflects the uncertainty associated with our estimates of past water content (Table 1, "F" column). For the other five samples, the combined systematic uncertainty essentially reflects the uncertainties associated with the calibration of the measurement facilities, the correction and conversion factors, and the cosmic dose rate, which all contribute approximately equally; it is only slightly higher than the combined random uncertainty. The total uncertainties on the ages for the samples collected from "L"-layers range from 11 to 18%, and are dominated by the random uncertainty associated with the measurement of D_e (see Fig. 5e–i,l).

The OSL ages (±1 sigma total uncertainty) for the samples obtained from "D" layers range from 0.08 ± 0.01 ka to 0.36 ± 0.05 ka. All ages are consistent with the stratigraphic position of the samples. The samples that were collected at the top of each profile (samples GLL-214313, -16, −20 and −25) yield the youngest ages. These ages are not entirely consistent within 2 sigma random uncertainty. There is, however, considerable variation in natural and saturated moisture contents (Table 1) suggesting that water content is, at least partially, a random source of uncertainty.

4.2. Anthracological analysis and radiocarbon dating

The charcoal assemblages of the kilns are dominated by Scots pine (*Pinus sylvestris*; 99.1%–100%) with a very small amount of common heather (*Calluna vulgaris*; 0.9%) in kiln 2567 (Table S1). From each of the kilns, a charred twig of Scots pine, with between two and six growth rings, was radiocarbon dated, except for kiln 2567 where the outer three growth rings from a larger branch were used for dating.

The conventional and calibrated ^{14}C dates are reported in Table S2. The dates for features 2557 (1661–1954 cal CE) and 2567 (1662–1953 cal CE) are similar and show wide age probability distributions. Two ^{14}C-dates were obtained for feature 2595. Within 95% probability, their ages barely overlap and cover an age range from 1510 cal CE to 1953 cal CE in total.

5. Discussion

Fig. 6 compares the calibrated ^{14}C-dates and the historical age information (December 1941– March/April 1942; see §2) with the nine OSL ages obtained for "D" samples from the three investigated features (§4.1.4). The OSL ages (with 2021 Common Era as year of reference) were recalculated as calendar dates (CE; Table 2, last column) and both the OSL and ^{14}C dates are expressed within 95.4% probability.

The ^{14}C dates for three of the charcoal samples are consistent with the independent age information. Their age probability distributions,

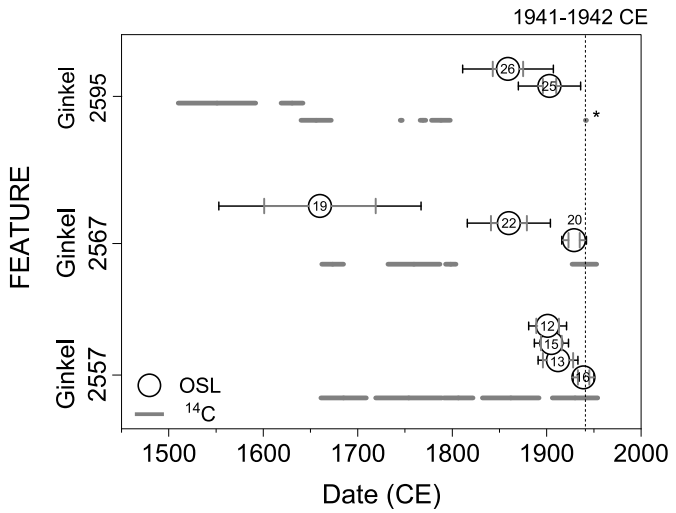

Fig. 6. Comparison between OSL ages, calibrated ^{14}C- ages, and historical evidence. Open circles represent OSL ages (with the black and grey error bars representing the total and random uncertainties, respectively), while grey solid bars show calibrated ^{14}C age ranges; both datasets cover 95.4% probability. The dashed line indicates the age (1941/1942 CE) of the kilns, which is known through historical sources (newspaper articles and photographs). All ages are expressed in years in Common Era (CE). The label "*" refers to the 1941–1942 CE (0.1%) and 1942–1953 (8.8%) probability intervals of the calibrated ^{14}C date for sample RICH-32218.

however, are very wide. The implication is that, in absence of other chronometric information, this method can only establish whether a feature is younger than 1650 CE; this is well-known (see §1). Moreover, the two inconsistent results obtained for feature 2595 are not understood, especially as both were obtained on the same taxon (*Pinus sylvestris*) and material (twig, 2 growth rings). This suggests that obtaining only a single ^{14}C-date for a kiln may lead to highly inaccurate interpretations. Indeed, the age of 1540–1642 cal CE (sample RICH-31549) is significantly older than the known age of 1941/1942 CE and must be considered an outlier. An old wood effect can be excluded as the sample consisted of a charred twig. There are also no indications in the stratigraphy of the kiln site for older charcoal production activities at the same location. Older residual charcoal that was present in the soil from previous (natural) fire events cannot completely be ruled out but it is unlikely that Scots pine was a substantial element in the vegetation in the area before c. 1650 CE (Van Mourik and Dijkstra, 1995; Maes et al., 2006). Given the wide age probability distributions, the ^{14}C-dates are also only of very limited use for assessing the accuracy of the OSL ages, which all indicate a post-1650 CE age for the kilns. The following therefore focusses on the comparison with the known age.

The optical ages for the uppermost samples collected from the "D" layers (samples −13, −16, −20 and −25) range from 1903 ± 33 CE to 1939 ± 11 CE. The OSL ages for the five samples collected from 5 cm lower at the base of the "D" layers are either similar (samples −12 and −15) or older (samples −19, −22 and −26). In combination with the generally apparent increase in spread in the D_e distributions with depth within the "D" layers (see §4.1.2; Fig. 5), one could thus argue that the four uppermost samples are most likely to date the event of interest. The ages of 1939 ± 11 and 1929 ± 13 (samples −16 and −20) are entirely consistent with the known age of 1941/1942 CE, while samples −13 and −25 yield slightly older dates of 1912 ± 21 CE and 1903 ± 33 CE, respectively.

Sample −13 exhibits a significantly higher spread in D_e (RSD of ~48 % compared to ~ 22–28% for the other three samples; Fig. 5a–c,d). At present, it is unknown whether this is a sample intrinsic characteristic or due to external factors (such as mixing and/or incomplete resetting). It can be noted that, within 2 sigma random uncertainties, its OSL age is

consistent with those obtained for samples −20 and −25 (Fig. 6; Table 2).

While the OSL ages for samples −13, −16, −20 and −25 are not entirely consistent within 2 sigma random uncertainties, our analysis does not allow preferring one result over another. If one would thus assume that the same event is dated by all four samples, an average age (±2 sigma total uncertainty; calculated following Aitken, 1985) of 0.094 ± 0.013 ka is obtained, i.e. 1928 ± 13 CE. Within uncertainty, this average date cannot be considered as inconsistent with the known age of 1941/1942 CE.

The 1 sigma overall (or total) uncertainty associated with the four individual OSL ages is approximately 7–14% (Table 2) and is 7% for their average age. Compared to ^{14}C, this is a significant improvement in the temporal resolution that can be achieved. Assuming that samples from different features within a given context can be dated with the same level of accuracy, and that the sources of systematic uncertainty are equally shared between these samples, opens up the possibility to relatively distinguish between features with a precision that is governed by random uncertainties only. For the four samples considered here, these are in the range of ~3–8% (Table 2); in case of distinguishing between different sets of coeval samples this could then be as low as 2% (i.e. the random uncertainty associated with the average age for samples −13, −16, −20 and −25, covering the three investigated features). However, for traces in contexts as investigated here (relic charcoal kilns), it is unlikely that all sources of systematic uncertainty (such as water content; see above and Table 1) will be equally shared, implying that the observed variability can be higher.

Finally, the comparison between the entire set of OSL ages and the known independent age control can inform about future strategies for collecting samples for OSL dating from relic charcoal kilns. It appears that samples taken from the top of the charcoal-rich layers are more likely to yield dates that accurately determine the time of charcoal production. These layers, however, can be considered as heterogenous in many ways and can often not unambiguously be delineated in field observations. In addition to significant variability in water content and porosity, the precise position of a profile pit (and hence of the targeted "D" layer and the exact sampling spot) within the kiln is often poorly constrained and may thus not necessarily be where heating was most stringent and resetting complete. In addition, it would seem likely that harvesting after production was probably more thorough in some parts than others, implying removal of the sediments that are most likely to have been fully reset; a sample may thus potentially contain a greater or smaller proportion of the underlying sediments. Our dataset may very well reflect such intricacies, demonstrating once more the added value of collecting multiple samples (incl. those for evaluating moisture content) from the same stratigraphic levels, as well as from vertical stratigraphic planes. The results then allow evaluating the internal consistency of the ages, which helps assessing their reliability.

6. Conclusions

We applied quartz-based OSL dating to sediments associated with three relic charcoal kilns for which the age is very well-constrained to December 1941 CE - March/April 1942CE. Four samples collected from the top of the charcoal-rich layers yielded the youngest OSL ages and, in combination with analysis of distributions of D_e, are thought to more likely approximate the time of charcoal production. While the results are not entirely consistent within 2 sigma random uncertainties, our analysis does not allow preferring one result over another. The four samples were therefore considered coeval, resulting in an average date (±2 sigma total uncertainty) of 1928 ± 13 CE. Taking this uncertainty into account, we conclude that this date is reasonably accurate. The precision associated with the individual OSL ages is in the range of 7–14% (1 sigma total uncertainty) and it might ideally be possible to establish relative chronologies within ~3–8%.

In general, we conclude that OSL dating can be particularly advantageous for resolving the chronometry of post-1650 CE charcoal kiln remains. The majority of the relic charcoal kilns in Europe date from exactly this period of time, for which ^{14}C cannot provide meaningful age information. Our study also highlights some intricacies, in particular with respect to water content and occasional radioactive disequilibrium. To fully assess the limits on precision and accuracy that these difficulties impose, more OSL dating studies of post-1650 CE relic charcoal hearths with a precisely known age are needed. Our finds suggest that such studies would then benefit from sampling at closely spaced vertical and horizontal intervals (≤5 cm) of both the dark charcoal-rich layers and the immediately over- and underlying sediments.

CRediT authorship contribution statement

Nasrin Karimi Moayed: Data curation, Formal analysis, Investigation, Software, Writing – original draft, Writing – review & editing, Visualization. **Dimitri Vandenberghe:** Conceptualization, Formal analysis, Investigation, Writing – review & editing. **Koen Deforce:** Data curation, Investigation, Formal analysis, Writing – review & editing. **Eva Kaptijn:** Investigation, Writing – review & editing. **Karsten Lambers:** Investigation, Writing – review & editing. **Wouter Verschoof-van der Vaart:** Investigation, Writing – review & editing. **Wim De Clercq:** Funding acquisition. **Johan De Grave:** Funding acquisition, Investigation, Project administration, Supervision, Writing – review & editing.

Declaration of competing interest

The authors declare that they have no known competing financial interests or personal relationships that could have appeared to influence the work reported in this paper.

Data availability

Data will be made available on request.

Acknowledgements

This research was partially funded by the UGent Special Research Fund, Interdisciplinary Research Project "Fueling the Furnace. An interdisciplinary study of forest soils as geoarchaeological archives." (BOF-IOP project 01IO3318) and by the Leiden University Fund for the project "Houtskoolmeilers: een vergeten ambacht op de Veluwe" (W20391-6-44). The utmost thanks is expressed to all volunteers of the Heritage Quest project who helped identify charcoal kilns on LiDAR images and assisted during the fieldwork.

Appendix A. Supplementary data

Supplementary data to this article can be found online at https://doi.org/10.1016/j.quageo.2024.101582.

References

Adamiec, G., Aitken, M.J., 1998. Dose-rate conversion factors: update. Ancient TL 16, 37–50.

Aitken, M.J., 1985. Thermoluminescence Dating. Academic Press, London, p. 359p. ISBN: 0-12-046380-6.

Boudin, M., Van Strydonck, M., Van Den Brande, T., Synal, H.A., Wacker, L., 2015. Rich - a new AMS facility at the royal Institute for cultural heritage, Brussels, Belgium. Nuclear Instruments and Methods in Physics Research, Section B: Beam Interactions with Materials and Atoms 361, 120–123. https://doi.org/10.1016/j.nimb.2015.04.006.

Deforce, K., Boeren, I., Adriaenssens, S., Bastiaens, J., De Keersmaeker, L., Haneca, K., Tys, D., Vandekerkhove, K., 2013. Selective woodland exploitation for charcoal production. A detailed analysis of charcoal kiln remains (ca. 1300-1900 AD) from Zoersel (northern Belgium). J. Archaeol. Sci. 40, 681–689. https://doi.org/10.1016/j.jas.2012.07.009.

Deforce, K., Groenewoudt, B., Haneca, K., 2021a. 2500 years of charcoal production in the Low Countries: the chronology and typology of charcoal kilns and their relation

with early iron production. Quat. Int. 593–594, 295–305. https://doi.org/10.1016/j.quaint.2020.10.020.
Deforce, K., Vanmontfort, B., Vandekerkhove, K., 2021b. Early and High Medieval (c. 650 AD - 1250 AD) charcoal production and its impact on woodland composition in the Northwest-European lowland: a study of charcoal pit kilns from Sterrebeek (Central Belgium). Environ. Archaeol. 26, 168–178. https://doi.org/10.1080/14614103.2018.1538087.
Duller, G.A.T., 2003. Distinguishing quartz and feldspar in single grain luminescence measurements. Radiat. Meas. 37, 161–165. https://doi.org/10.1016/S1350-4487(02)00170-1.
Foster, D., Swanson, F., Aber, J., Burke, I., Brokaw, N., Tilman, D., Knapp, A., 2003. The importance of land-use legacies to ecology and conservation. Bioscience 53, 77–88. https://doi.org/10.1641/0006-3568(2003)053[0077:TIOLUL]2.0.CO;2.
Gale, R., 2003. Wood-based industrial fuels and their environmental impact in lowland britain. In: Murphy, P., Wiltshire, P.E.J. (Eds.), The Environmental Archaeology of Industry. Symposia of the Association for Environmental Archaeology, 20. Oxford: Oxford Books, pp. 30–47.
Groenewoudt, B., Spek, T., 2016. Woodland dynamics as a result of settlement relocation on Pleistocene sandy soils in The Netherlands (200 BC–AD 1400). Rural Landscapes: Society, Environment, History 3, 1–17. https://doi.org/10.16993/rl.20.
Hardy, B., Dufey, J.E., 2012. Estimation des besoins en charbon de bois et en superficie forestière pour la sidérurgie wallonne préindustrielle (1750-1830). Deuxième partie: les besoins en superficie forestière. Rev. For. Fr. (Nancy). https://doi.org/10.4267/2042/48747.
Hesse, R., 2010. LiDAR-derived Local Relief Models – a new tool for archaeological prospection. Archaeol. Prospect. 17, 67–72. https://doi.org/10.1002/arp.374.
Hossain, S.M., 2003. A Critical Comparison and Evaluation of Methods for the Annual Radiation Dose Determination in the Luminescence Dating of Sediments. Ph.D. thesis. Ghent University.
Karimi-Moayed, N., Vandenberghe, D.A.G., Deforce, K., Bastiaens, J., Ghyselbrecht, E., Debeer, A.E., De Smedt, P., De Clercq, W., De Grave, J., 2020. Bypassing the Suess-effect: age determination of charcoal kiln remains using OSL dating. J. Archaeol. Sci. 120, 105176 https://doi.org/10.1016/j.jas.2020.105176.
Karimi-Moayed, N., Vandenberghe, D.A.G., Buylaert, J.-P., Deforce, K., Debeer, A.-E., Biernacka, P., De Smedt, P., De Clercq, W., De Grave, J., 2022. A combined OSL and 14C dating study of charcoal production in the sandy environment of Zoersel forest (N Belgium). Quat. Geochronol. 71, 101339 https://doi.org/10.1016/j.quageo.2022.101339.
Karimi-Moayed, N., Vandenberghe, D.A.G., Deforce, K., Kaptijn, E., Biernacka, P., De Clercq, W., De Grave, J., 2023. OSL dating as an alternative tool for age determination of relic charcoal kilns. Archaeometry 1–16. https://doi.org/10.1111/arcm.12860. February 2023.
Karimi-Moayed, N., 2023. Testing the Potential of OSL Dating for Application to Heated Anthropogenic Sediments (Hearth and Charcoal Kiln Remains). Ghent University. Faculty of Sciences. http://hdl.handle.net/1854/LU-01H4FYKPNBG95NEDNDX9YD54PQ.
Lepper, K., Larsen, N.A., McKeever, S.W.S., 2000. Equivalent dose distribution analysis of Holocene eolian and fluvial quartz sands from Central Oklahoma. Radiat. Meas. 32, 603–608. https://doi.org/10.1016/S1350-4487(00)00093-7.
Ludemann, T., 2003. Large-scale reconstruction of ancient forest vegetation by anthracology - a contribution from the Black Forest. Phytocoenologia 33 (4), 645–666. https://doi.org/10.1127/0340-269X/2003/0033-0645.
Ludemann, T., 2010. Past fuel wood exploitation and natural forest vegetation in the Black Forest, the Vosges and neighbouring regions in western Central Europe. Palaeogeogr. Palaeoclimatol. Palaeoecol. 291, 154–165. https://doi.org/10.1016/j.palaeo.2009.09.013.
Madsen, A.T., Murray, A.S., Andersen, T.J., Pejrup, M., Breuning-Madsen, H., 2005. Optically stimulated luminescence dating of young estuarine sediments: a comparison with ^{210}Pb and ^{137}Cs dating. Mar. Geol. 214, 251–268. https://doi.org/10.1016/j.margeo.2004.10.034.
Maes, B., Bastiaens, J., Brinkkemper, O., Deforce, K., Rövekamp, C., Van Den Bremt, P., Zwaenepoel, A., 2006. Inheemse bomen en struiken in Nederland en Vlaanderen (Amsterdam, Boom).
Mejdahl, V., 1979. Thermoluminescence dating: beta-dose attenuation in quartz grains. Archaeometry 21, 61–72.
Murray, A.S., Wintle, A.G., 2000. Luminescence dating of quartz using an improved single-aliquot regenerative-dose protocol. Radiat. Meas. 32, 57–73. https://doi.org/10.1016/S1350-4487(99)00253-X.
Murray, A.S., Wintle, A.G., 2003. The single aliquot regenerative dose protocol: potential for improvements in reliability. Radiat. Meas. 37, 377–381. https://doi.org/10.1016/S1350-4487(03)00053-2.
Nelle, O., 2003. Woodland history of the last 500 years revealed by anthracological studies of charcoal kiln sites in the Bavarian Forest, Germany. Phytocoenologia 33, 667–682. https://doi.org/10.1127/0340-269X/2003/0033-0667.
Olesen, M.W., 2019. Iron smelting during the late iron age in central jutland. In: A Stamnes, A., Risbol, O., Stenvik, L.F. (Eds.), Investigating Early Iron Production by Modern Remote Sensing Technologies, Vols. 2–2019. The Royal Norwegian Society of Sciences and Letters, pp. 17–33.
Olley, J.M., Murray, A.S., Roberts, R.G., 1996. The effects of disequilibria in the uranium and thorium decay chains on burial dose rates in fluvial sediments. Quat. Sci. Rev. 15, 751–760. https://doi.org/10.1016/0277-3791(96)00026-1.
Prescott, J.R., Hutton, J.T., 1994. Cosmic ray contributions to dose rates for luminescence and ESR dating: large depths and long-term time variations. Radiat. Meas. 23, 497–500. https://doi.org/10.1016/1350-4487(94)90086-8.
Raab, A., Takla, M., Raab, T., Nicolay, A., Schneider, A., Rösler, H., Heussner, K.-U., Bönisch, E., 2015. Pre-industrial charcoal production in Lower Lusatia (Brandenburg, Germany): detection and evaluation of a large charcoal-burning field by combining archaeological studies, GIS-based analyses of shaded-relief maps and dendrochronological age determination. Quat. Int. 367, 111–122. https://doi.org/10.1016/j.quaint.2014.09.041.
Reimer, P.J., Austin, W., Bard, E., Bayliss, A., Blackwell, P., Bronk Ramsey, C., Butzin, M., Cheng, H., Edwards, R., Friedrich, M., Grootes, P., Guilderson, T., Hajdas, I., Heaton, T., Hogg, A., Hughen, K., Kromer, B., Manning, S., Muscheler, R., Palmer, J., Pearson, C., van der Plicht, J., Reimer, R., Richards, D., Scott, E., Southon, J., Turney, C., Wacker, L., Adolphi, F., Büntgen, U., Capano, M., Fahrni, S., Fogtmann-Schulz, A., Friedrich, R., Köhler, P., Kudsk, S., Miyake, F., Olsen, J., Reinig, F., Sakamoto, M., Sookdeo, A., Talamo, S., 2020. The IntCal20 Northern Hemisphere radiocarbon age calibration curve (0–55 cal kBP). Radiocarbon 62.
Reimer, R.W., Reimer, P.J., 2023. CALIBomb [WWW program] at. http://calib.org/CALIBomb/. (Accessed 11 November 2023).
Rutkiewicz, P., Malik, I., Wistuba, M., Sady, A., 2017. Charcoal kilns as a source of data on the past iron industry (an example from the River Czarna valley, Central Poland). Environmental & Socio-economic Studies 5, 12–22. https://doi.org/10.1515/environ-2017-0012.
Schoch, W., Heller, I., Schweingruber, F.H., Kienast, F., 2004. Wood anatomy of central European Species. Online version: www.woodanatomy.
Stuiver, M., 1961. Variations in radiocarbon concentration and sunspot activity. Geophysical Research 66, 273–276. https://doi.org/10.1029/JZ066i001p00273.
Tans, P.P., De Jong, A.F.M., Mook, W.G., 1979. Natural atmospheric ^{14}C variation and the Suess effect. Nature 280, 826–828. https://doi.org/10.1038/280826a0.
Van Mourik, J.M., Dijkstra, E.F., 1995. Geen inheemse dennen rond de Oisterwijkse vennen. Nederl. Bosbouwtijdschrift 67, 51–59.
Vandenberghe, D., De Corte, F., Buylaert, J.P., Kučera, J., Van den haute, P., 2008. On the internal radioactivity in quartz. Radiat. Meas. 43, 771–775. https://doi.org/10.1016/j.radmeas.2008.01.016.
Willis, K.J., Birks, H.J.B., 2006. What is natural? The need for a long-term perspective in biodiversity conservation. Science 314, 1261–1265.
Vandenberghe, D., 2004. Investigation of the optically stimulated luminescence dating method for application to young geological dediments. PhD thesis, Universiteit Gent, 358p.